

# Alloyed Crystalline CdSe<sub>1-x</sub>S<sub>x</sub> Semiconductive Nanomaterials – A Solid State <sup>113</sup>Cd NMR Study

Baoyan Xing,<sup>[a, b]</sup> Sai Ge,<sup>[b]</sup> Jianguo Zhao,<sup>\*[a, b]</sup> Hui Yang,<sup>[b]</sup> Jie Song,<sup>[b]</sup> Yu Geng,<sup>[b]</sup> Yuying Qiao,<sup>[b]</sup> Ling Gu,<sup>[b]</sup> Peide Han,<sup>\*[a]</sup> and Guibin Ma<sup>\*[b]</sup>

Solid-state NMR analysis on wurtzite alloyed CdSe<sub>1-x</sub>S<sub>x</sub> crystalline nanoparticles and nanobelts provides evidence that the <sup>113</sup>Cd NMR chemical shift is not affected by the varying sizes of nanoparticles, but is sensitive to the S/Se anion molar ratios. A linear correlation is observed between <sup>113</sup>Cd NMR chemical shifts and the sulfur component for the alloyed CdSe<sub>1-x</sub>S<sub>x</sub> (0 < x < 1) system both in nanoparticles and nanobelts ( $\delta_{\text{Cd}} = 169.71 \cdot X_{\text{S}} + 529.21$ ). Based on this correlation, a rapid and

applied approach has been developed to determine the composition of the alloyed nanoscalar materials utilizing <sup>113</sup>Cd NMR spectroscopy. The observed results from this system confirm that one can use <sup>113</sup>Cd NMR spectroscopy not only to determine the composition but also the phase separation of nanomaterial semiconductors without destruction of the sample structures. In addition, some observed correlations are discussed in detail.

## 1. Introduction


High-quality colloidal, single crystalline semiconductor nanoparticles (well known as quantum dots, QD) exhibit size-dependent optoelectronic properties, and have generated interest from both a fundamental science and a technological perspective.<sup>[1-5]</sup> Therefore, their properties are currently under intensive study for diverse applications such as nanoelectronic devices, QD lasers, biosensing, and biolabeling.<sup>[6-12]</sup> Recent advances have led to the development of core-shell QDs,<sup>[13-15]</sup> doped magnetic nanoparticles,<sup>[16-18]</sup> and QD quantum-well heterostructures.<sup>[19-20]</sup> As an alternative to tuning the electronic, optical, and magnetic properties by varying the size of the nanoparticles it is also possible to alter the composition of the nanoparticles. Many studies have focused on tuning nanoparticle properties by changing the composition. The ternary alloyed semiconductor nanoparticles, such as CdSeTe,<sup>[21]</sup> CdSeS,<sup>[22]</sup> ZnCdSe,<sup>[23]</sup> and ZnCdS,<sup>[24]</sup> have been synthesized and the dependence of properties on composition has been demonstrated.


A typical synthesis method used to generate QDs in solution is a colloidal nucleation process. As is known from the thermodynamic equilibrium constants, the nucleus formation order differs vastly between differing cation and anion pairs (e.g.  $K_{\text{CdS}} < K_{\text{CdSe}}$ ). This difference makes the alloyed nucleation process more complicated and the composition uncertain. It therefore is essential to develop a non-destructive analytical approach to determine the precise composition of nanoparticles. NMR spectroscopy is a technique whereby the nucleus being probed is sensitive to its local chemical and electronic environments and therefore may be complementary to other characterization techniques, such as X-ray diffraction and optical spectroscopy. Thus, NMR spectroscopy may provide additional information such as identifying the different environments of the studied nucleus.

NMR techniques have previously been successfully applied in the investigation of semiconductor nanomaterials.<sup>[25]</sup> Douglass *et al.* have measured three sizes of CdSe nanoparticles by <sup>77</sup>Se NMR,<sup>[26]</sup> and Vega *et al.* have studied the surface properties of precipitated nanoparticles of CdS by <sup>113</sup>Cd NMR.<sup>[27]</sup> From the available literature, a couple of research groups, e.g. Alivisatos and Strouse, have studied the nanoparticles of InP by <sup>31</sup>P NMR spectroscopy and of CdSe by <sup>113</sup>Cd and <sup>77</sup>Se NMR spectroscopy.<sup>[28-40]</sup> Very recently, M. V. Kovalenko *et al.* have applied dynamic nuclear polarization (DNP) surface enhanced NMR spectroscopy to study the structures of InP and CdSe colloidal quantum dots (QDs); this technique makes it more efficient to study their cores, surfaces and capping ligands.<sup>[41-42]</sup> In this study, we have systemically synthesized different compositions of alloyed ternary CdSe<sub>1-x</sub>S<sub>x</sub> nanoparticles and nanobelts and used these systems for the indirect quantitative determination of alloyed nanoparticle compositions via <sup>113</sup>Cd NMR spectroscopy.

[a] Dr. B. Xing, Prof. J. Zhao, Prof. P. Han  
College of Materials Science and Engineering  
Taiyuan University of Technology  
Taiyuan 030024 (China)  
E-mail: jgzhao@163.com  
hanpeide@126.com

[b] Dr. B. Xing, Dr. S. Ge, Prof. J. Zhao, Dr. H. Yang, Dr. J. Song, Dr. Y. Geng,  
Dr. Y. Qiao, Prof. L. Gu, Prof. G. Ma  
Institute of Carbon Materials Science  
Shanxi Datong University  
Datong 037009 (China)  
E-mail: jgzhao@163.com  
guibin@ualberta.ca

 Supporting information for this article is available on the WWW under <https://doi.org/10.1002/open.202000216>

 © 2020 The Authors. Published by Wiley-VCH GmbH. This is an open access article under the terms of the Creative Commons Attribution Non-Commercial NoDerivs License, which permits use and distribution in any medium, provided the original work is properly cited, the use is non-commercial and no modifications or adaptations are made.

## 2. Results and Discussion

### 2.1. CdSe<sub>1-x</sub>S<sub>x</sub> Nanoparticles

Four samples of a wurtzite hexagonal structure of the alloyed ternary nanocrystals of CdSe<sub>1-x</sub>S<sub>x</sub> ( $0 < x < 1$ ) were synthesized and their apparent compositions were determined by ICP mass

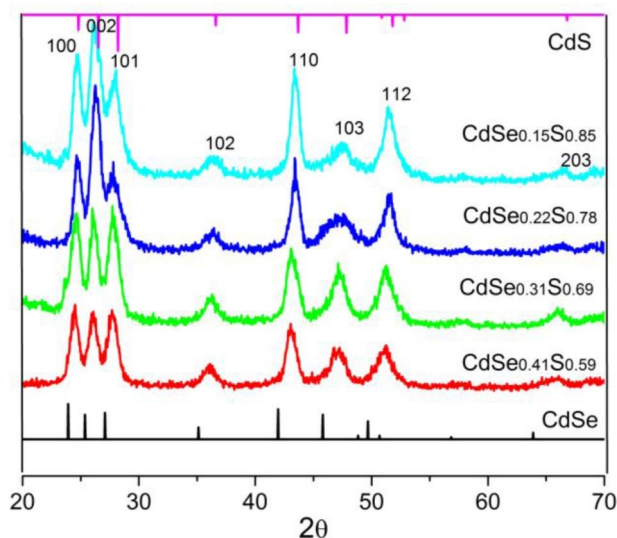


**Figure 1.** XRD patterns for CdSe<sub>1-x</sub>S<sub>x</sub> ( $0 < x < 1$ ) nanoparticles with various (S/Se) molar ratios.

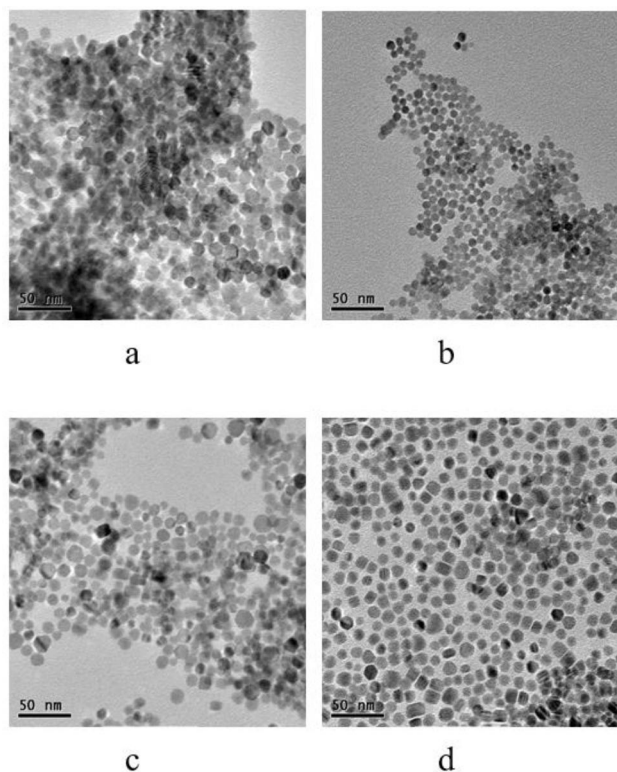


**Figure 2.** TEM images of (a) CdSe<sub>0.41</sub>S<sub>0.59</sub>, (b) CdSe<sub>0.31</sub>S<sub>0.69</sub>, (c), CdSe<sub>0.22</sub>S<sub>0.78</sub> and (d) CdSe<sub>0.15</sub>S<sub>0.85</sub>.

as shown in Figure 1. The XRD patterns exhibit seven prominent peaks related to the scattering planes as noted in Figure 1. The XRD peaks gradually shift to large angles as the sulfur content increases. No phase separation diffraction peaks of individual phases for CdSe and CdS were detected in the XRD spectra, indicating that a homogeneous alloyed nanoparticle phase of CdSe<sub>1-x</sub>S<sub>x</sub> was formed. The transmission electron microscopy (TEM) images of the four synthesized samples demonstrate that they are uniform mono-dispersed nanoparticles and that their diameters are almost identical (Figure 2).

### 2.2. CdSe<sub>1-x</sub>S<sub>x</sub> Nanobelts

Hydrothermal synthesis of alloyed CdSe<sub>1-x</sub>S<sub>x</sub> nanomaterials in neat ethylenediamine is straightforward and the formed products show different colors for different molar fractions of sulfur and selenium, from yellow to black (Figure 3). The synthesis reaction is near quantitative with yields of all four preparations reaching 93–98%; elemental analysis showed that the compositions agree with our expected results (Table 1). The XRD patterns are similar to those for the CdSe<sub>1-x</sub>S<sub>x</sub> nanoparticles; all are in a wurtzite hexagonal structure (SI, Figure S1). SEM shows they are all nanobelts with lengths of a few micrometers (Figure 3).

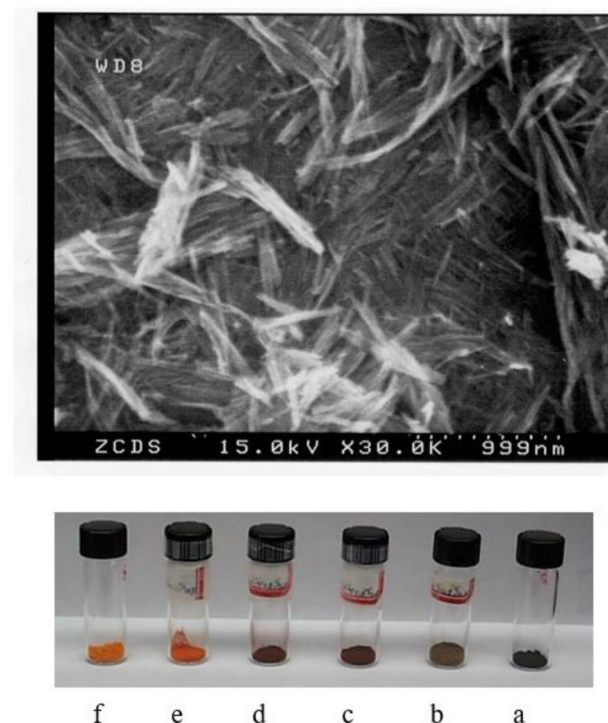


**Figure 3.** SEM images of CdSe<sub>0.5</sub>S<sub>0.5</sub> nanobelts (top) and their colors (bottom). a, b, c, d, e and f represents the color of different compositions of nanobelts shown in Figure 6. a: CdSe/CdSe<sub>1.0</sub>S<sub>0.0</sub>, b: CdSe<sub>0.8</sub>S<sub>0.2</sub>, c: CdSe<sub>0.6</sub>S<sub>0.4</sub>, d: CdSe<sub>0.5</sub>S<sub>0.5</sub>, e: CdSe<sub>0.2</sub>S<sub>0.8</sub>, and f: CdS/CdSe<sub>0.0</sub>S<sub>1.0</sub>.

| Table 1. Experimental details of synthesis and elemental analysis results for the CdSe <sub>1-x</sub> S <sub>x</sub> (0 < x < 1) systems. |  |  |  |  |
|---|--|--|--|--|
| Nanoparticles (mixed millimoles of chemical precursors)   |  |  |  |  |
| S   | 4.8                                    | 5.0                                    | 5.2                                    | 4.8                                    |
| Se  | 0.6                                    | 0.5                                    | 0.4                                    | 0.3                                    |
| CdO   | 1.2                                    | 1.2                                    | 1.2                                    | 1.2                                    |
| E.A. results  | CdSe <sub>0.41</sub> S <sub>0.59</sub> | CdSe <sub>0.31</sub> S <sub>0.69</sub> | CdSe <sub>0.22</sub> S <sub>0.78</sub> | CdSe <sub>0.15</sub> S <sub>0.85</sub> |
| Nanobelts (mixed millimoles of chemical precursors)   |  |  |  |  |
| S   | 0.2                                    | 0.4                                    | 0.5                                    | 0.8                                    |
| Se  | 0.8                                    | 0.6                                    | 0.5                                    | 0.2                                    |
| Cd(ClO <sub>4</sub> ) <sub>2</sub>  | 1.0                                    | 1.0                                    | 1.0                                    | 1.0                                    |
| Yield (%)   | 94.5                                   | 92.5                                   | 93.3                                   | 97.4                                   |
| Supposed  | CdSe <sub>0.8</sub> S <sub>0.2</sub>   | CdSe <sub>0.6</sub> S <sub>0.4</sub>   | CdSe <sub>0.5</sub> S <sub>0.5</sub>   | CdSe <sub>0.2</sub> S <sub>0.8</sub>   |
| E.A. results  | CdSe <sub>0.80</sub> S <sub>0.19</sub> | CdSe <sub>0.58</sub> S <sub>0.39</sub> | CdSe <sub>0.48</sub> S <sub>0.50</sub> | CdSe <sub>0.20</sub> S <sub>0.80</sub> |

### 2.3. T<sub>1</sub> Measurements

To obtain quantitative information from the <sup>113</sup>Cd NMR spectra, the recycle delay should be at least five times greater than the longest <sup>113</sup>Cd T<sub>1</sub> (*i. e.*,  $t > 5T_1$ ). Therefore, the <sup>113</sup>Cd NMR T<sub>1</sub> values for CdS, CdSe, and CdTe bulk powders, as well as for one nanobelt sample, CdSe<sub>0.5</sub>S<sub>0.5</sub> (*i. e.*,  $x = 0.5$ ), were measured using the saturation recovery technique (data see Table 2). The results show that the <sup>113</sup>Cd T<sub>1</sub> of bulk powders dramatically increases through the series S, Se, Te with that for the CdSe<sub>0.5</sub>S<sub>0.5</sub> nanobelts falling in between those for CdSe and CdTe. These results show that they all have very long T<sub>1</sub> values in solid bulk phases and even longer in the nano phase such as in nanobelt materials (data in Table 2 and details in SI, Figure S2).

The magnetically active isotopes of cadmium, <sup>111</sup>Cd and <sup>113</sup>Cd, have nuclear spin ( $I = 1/2$ ) and thus do not experience electric quadrupole interactions. All the possible relaxation mechanisms for these nuclei are therefore of magnetic origin; *i. e.*, the spin systems achieve thermal equilibrium with the lattice as a result of transitions (spin flips) induced by local, fluctuating magnetic fields at the nuclear sites. The energy gaps

| Table 2. <sup>113</sup> Cd chemical shifts and T <sub>1</sub> values for alloyed CdSe <sub>1-x</sub> S <sub>x</sub> (0 < x < 1) nanomaterials and related bulk powders. |                            |                    |  |
|---|----------------------------|--------------------|--|
| Chemicals   | <sup>113</sup> Cd CS [ppm] | T <sub>1</sub> [s] | Literature data <sup>[46]</sup> CS (ppm) |
| Individual phase  |                            |                    |  |
| Cd-Octadecene   | -60.5 (0.1)                |                    |  |
| CdO   | 382.0 (0.1)                |                    |  |
| CdTe  | 273.0 (0.1)                | 385.4 (0.1)        | 283.0                                    |
| CdSe  | 532.0 (0.1)                | 185.6 (0.1)        | 550.0                                    |
| CdS   | 697.6 (0.1)                | 36.0 (0.1)         | 692.0                                    |
| Nanobelts   |                            |                    |  |
| CdSe <sub>0.8</sub> S <sub>0.2</sub>  | 558.0 (0.2)                |                    |  |
| CdSe <sub>0.6</sub> S <sub>0.4</sub>  | 591.0 (0.2)                | 238.8 (0.1)        |  |
| CdSe <sub>0.5</sub> S <sub>0.5</sub>  | 624.0 (0.2)                |                    |  |
| CdSe <sub>0.2</sub> S <sub>0.8</sub>  | 662.0 (0.2)                |                    |  |
| Nanoparticles   |                            |                    |  |
| CdSe <sub>0.41</sub> S <sub>0.59</sub>  | 630.0 (0.2)                |                    |  |
| CdSe <sub>0.31</sub> S <sub>0.69</sub>  | 646.0 (0.2)                |                    |  |
| CdSe <sub>0.22</sub> S <sub>0.78</sub>  | 658.0 (0.2)                |                    |  |
| CdSe <sub>0.15</sub> S <sub>0.85</sub>  | 674.0 (0.2)                |                    |  |

of the semiconductors increase in the order of CdTe < CdSe < CdS, which is the same order as our measured longitudinal relaxation rates. This clearly indicates that the short <sup>113</sup>Cd T<sub>1</sub> values correlate with a high energy gap. A linear correlation was found between the measured <sup>113</sup>Cd T<sub>1</sub> of each CdS, CdSe and CdTe individual bulk semiconductor material and its corresponding chemical shift (SI, Figure S3).

### 2.4. <sup>113</sup>Cd NMR Chemical Shifts of Nanoparticles

In a typical colloidal synthesis, one often controls nanoparticle sizes by varying the nucleation times. We have measured the <sup>113</sup>Cd NMR chemical shifts of four alloyed CdSe<sub>1-x</sub>S<sub>x</sub> nanoparticle samples as a function of reaction time or nanoparticle diameter, all of which had the same initial composition (molar ratio of Cd:S:Se = 1.0:4.2:0.3), but prepared with different nucleation times (10, 30, 60 and 240 minutes). Identical <sup>113</sup>Cd NMR chemical shifts were obtained for all four samples (Figure 4), indicating that the chemical shift is not affected by varying the diameters of the nanoparticles. This behavior was also proved by measuring the NMR chemical shifts of three different sizes of CdSe nanoparticles. <sup>113</sup>Cd NMR spectra of three different diameters of CdSe nanoparticles (3.6 nm, absorption at 532 nm; 4.5 nm, absorption at 562 nm; 8.0 nm, absorption at 642 nm) have been measured (SI, Figure S4 and Figure S4 (continue)). The spectra show that the chemical shifts are not sensitive to the nanoparticle sizes. The results clearly show that <sup>113</sup>Cd NMR chemical shifts do not change with changing CdSe nanoparticle diameters. However, the <sup>113</sup>Cd chemical shifts did change as a function of composition. For the four different compositions of alloyed CdSe<sub>1-x</sub>S<sub>x</sub> nanoparticles, the <sup>113</sup>Cd NMR spectra show a broad symmetric signal for each individual, and it shifted to higher ppm values with increased sulfur content. <sup>113</sup>Cd NMR chemical shifts ( $\delta_{\text{Cd}}$ ) correlate (Figure 5) to the sulfur molar fraction (X<sub>S</sub>).

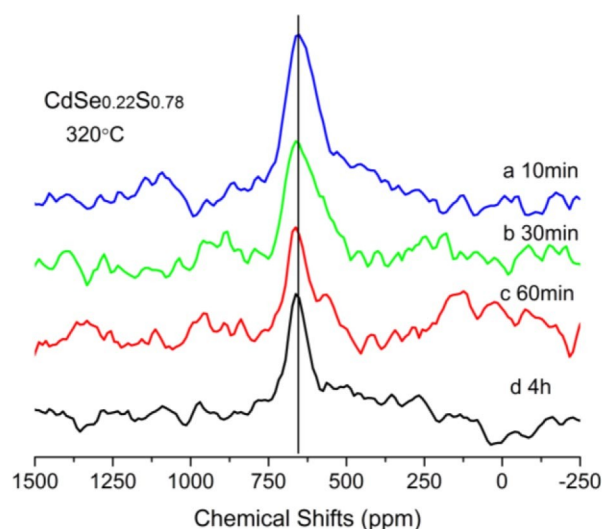
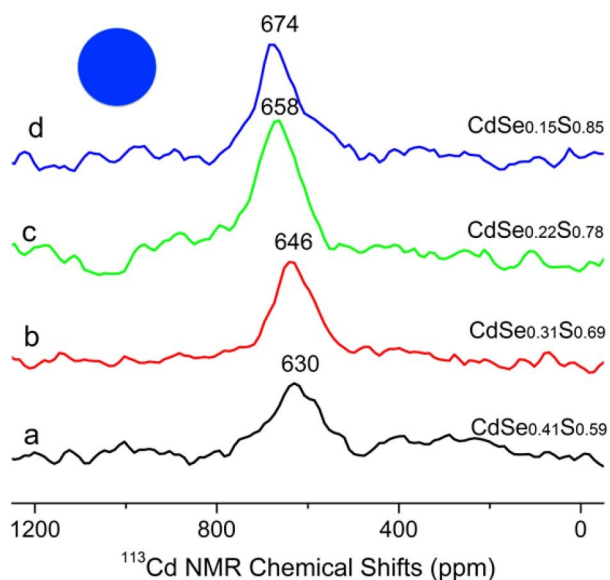
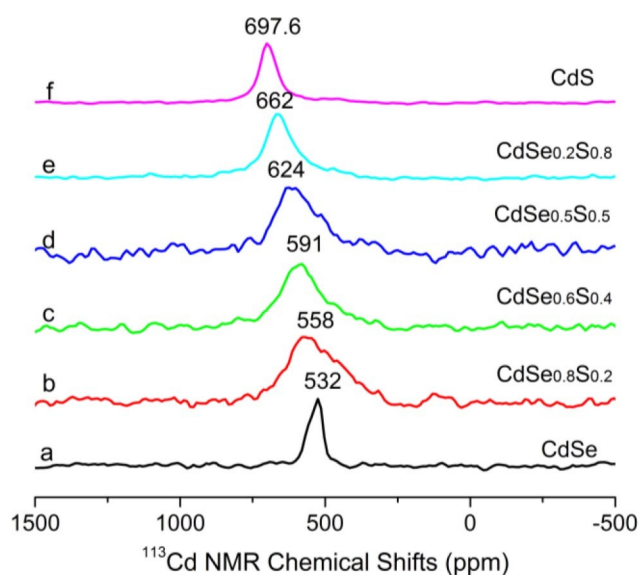


Figure 4. <sup>113</sup>Cd NMR spectra of CdSe<sub>0.22</sub>S<sub>0.78</sub> nanoparticles prepared with different nucleation times (a: 10 minutes, b: 30 minutes, c: 60 minutes and d: 4 hours).



**Figure 5.**  $^{113}\text{Cd}$  NMR spectra for different compositions of alloyed  $\text{CdSe}_{1-x}\text{S}_x$  nanoparticles in the solid state. These four samples XRD (as shown in Figure 1) and TEM images (as shown in Figure 2). XRD show the similar line widths and the diffraction peaks are slightly shift to CdS peak position and TEM images measured these four samples of nanoparticles diameters are a):  $8.76 \pm 1.27$  nm; b):  $7.49 \pm 1.09$  nm; c):  $9.48 \pm 2.06$  nm; and d):  $9.39 \pm 1.71$  nm (details in Figure S14 in SI).

To further elucidate this correlation, alloyed  $\text{CdSe}_{1-x}\text{S}_x$  nanobelts of precise compositions were synthesized using the hydrothermal method in a neat ethylenediamine solution.  $^{113}\text{Cd}$  NMR spectra of all the samples were obtained (Figure 6) and they present a very good linear correlation with the sulfur mole fraction (Figure 7). Equation (1) was obtained through a linear



**Figure 6.**  $^{113}\text{Cd}$  NMR spectra of different composition of alloyed  $\text{CdSe}_{1-x}\text{S}_x$  nanobelts in the solid state (each sample shows a different color; see Figure 3).

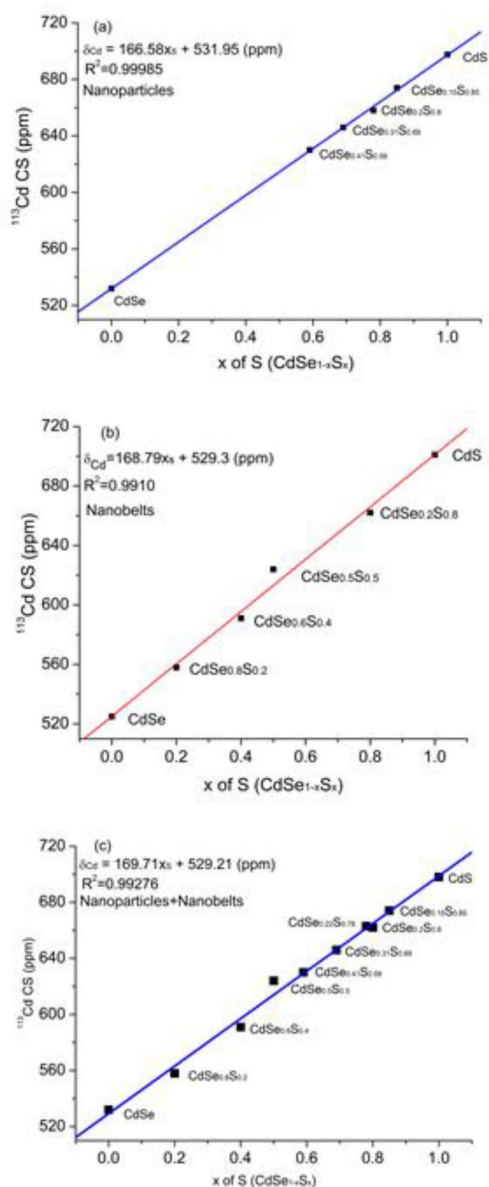


**Figure 7.** Linear correlations between  $^{113}\text{Cd}$  NMR chemical shifts and the sulfur molar fraction ( $x$ ) for  $\text{CdSe}_{1-x}\text{S}_x$  ( $0 < x < 1$ ) (a) nanoparticles, (b) nanobelts and (c) for all data from both nanoparticles and nanobelts.

fit of all the experimental data from both nanoparticles and nanobelts.

$$\delta_{\text{Cd}} = 169.71 \cdot x_{\text{S}} + 529.21 \quad (1)$$

Thus, based on Equation (1), the composition formulas ( $x$ ) for any synthesized type of  $\text{CdSe}_{1-x}\text{S}_x$  alloyed semiconductor material, including alloyed nanoparticles, can be determined by measuring their  $^{113}\text{Cd}$  NMR chemical shifts.



## 2.5. Chemical Shifts

In principle, the Ramsey equation describes the chemical shift for an atom A ( $\delta_A$ ) as composed of two terms, diamagnetic ( $\delta_{\text{dia}}$ ) and paramagnetic ( $\delta_{\text{para}}$ ).<sup>[43]</sup> The diamagnetic contribution ( $\delta_{\text{dia}}$ ) is mainly due to the core electrons and can determine the chemical shifts of the lightest nuclei. For heavier nuclei, this diamagnetic contribution remains essentially constant and the paramagnetic term determines the chemical shifts.<sup>[44]</sup> For the late transition elements, an ab initio study of metal nuclei chemical shifts in complexes of Cu, Ag, Cd and Zn concluded that for contributions to  $\delta_{\text{para}}$  the *d* mechanism is predominant for Cu, the shielding decreasing with increase in  $\pi(\text{M} \rightarrow \text{L})$  charge transfer as  $\text{Cl} < \text{NH}_3 < \text{CN}$ , whereas the *p* mechanism is dominant for Zn and Cd, with the shielding decreasing with decreasing ligand electronegativity, as  $\text{H}_2\text{O} > \text{Cl} > \text{CH}_3$ .<sup>[45]</sup> Very recently, M. V. Kovalenko *et al.*<sup>[42]</sup> applied DFT calculations to elucidate the magnetic shielding of cadmium in  $[\text{Cd}(\text{XH}_2)_{4-n}(\text{YH}_2)_n]^{2+}$  complexes (X, Y=O, S, Se and Te). Four different contributions (diamagnetic ( $\sigma_{\text{dia}}$ ), paramagnetic ( $\sigma_{\text{para}}$ ), spin-orbital ( $\sigma_{\text{so}}$ ) and isotropic ( $\sigma_{\text{iso}}$ )) to the magnetic shielding of cadmium are explored individually and their sum contributions relative to the  $^{113}\text{Cd}$  shielding of  $[\text{Cd}(\text{OH}_2)_4]^{2+}$ . The calculated results also indicate that the shielding to the bonding central Cd nuclei is in the atomic order  $\text{O} > \text{S} > \text{Se} > \text{Te}$  which is also consistent with this electronegativity model.<sup>[42]</sup> Therefore, we can conclude that metal chemical shifts are primarily due to the metal *p* and *d* orbital contributions by the donation of electrons from the ligands to the metal outer *p* orbitals and by the back-donation of electrons from the metal *p* orbital to the ligands. In other words, the electrons in the outer *p* orbitals and the holes in the valence *d* orbitals produce the metal chemical shifts. In principle, this model can be used here to explain the observed  $^{113}\text{Cd}$  chemical shifts. The electronegativity of S, Se and Te is 2.589, 2.424 and 2.158 respectively. The ability of donating electrons to the Cd(II) outer *p* orbitals and withdrawing electrons from the Cd(II) valence *d* orbitals is proportional to the bonding elemental electronegativity.  $^{113}\text{Cd}$  chemical shifts for CdS, CdSe and CdTe were reported early in the literature,<sup>[46]</sup> and we have measured the  $^{113}\text{Cd}$  NMR chemical shifts of CdS, CdSe and CdTe under the same conditions (Table 2); the experimental data is very close to that reported in the literature. The  $^{113}\text{Cd}$  NMR chemical shifts of CdS, CdSe and CdTe fit very well to the electronegativity model. A linear plot was obtained between the electronegativity of S, Se and Te elements and their  $^{113}\text{Cd}$  chemical shifts (SI, Figure S5). This model is applied to evaluate our measured chemical shifts of alloyed  $\text{CdSe}_{1-x}\text{S}_x$  nanomaterials. The plot of  $^{113}\text{Cd}$  chemical shifts vs. summation of all anion elemental electronegativity contributions around the Cd nuclei ( $x\text{EN}_S + (1-x)\text{EN}_{\text{Se}}$ , where *x* is the sulfur fraction of the alloyed nanoparticles) exhibits a good linear correlation and fit this model very well (Figure 8). Such a correlations has been observed in  $\text{ZnX}_4^{2-}$ ,  $\text{CdX}_4^{2-}$ ,<sup>[47-51]</sup>  $\text{PtX}_6^{2-}$  and  $\text{PtX}_4^{2-}$ <sup>[52-59]</sup> halide complexes (X=F, Cl, Br and I) and a similar linear dependence has also found in the Cd(II)<sup>[60]</sup> and Tl(III) nitrogen and oxygen donor ligand complexes in solution.<sup>[61-62]</sup> In the DFT calculations on  $[\text{Cd}(\text{XH}_2)_4]^{2+}$  (X=O, S, Se and Te) by M. V. Kovalenko *et al.*

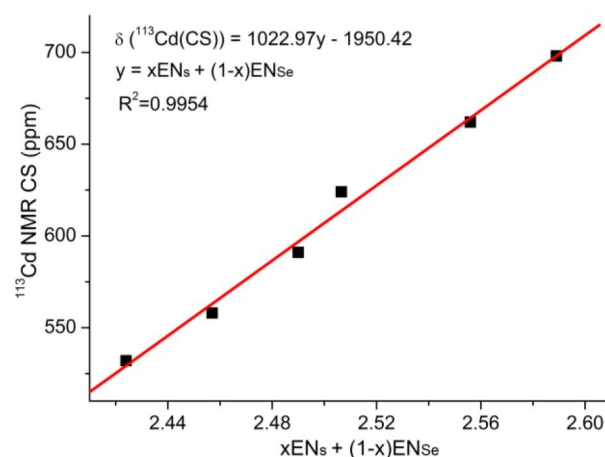


**Figure 8.** Linear correlation between EN of alloyed  $\text{CdSe}_{1-x}\text{S}_x$  nanoparticles and  $^{113}\text{Cd}$  NMR chemical shifts.

discussed above, a linear behavior when gradually exchanging of chalcogenide ions around cadmium cations was found.<sup>[42]</sup> The chemical shift of cadmium coordinating to sulfur and selenium atoms thus approximately corresponds to a weighted linear combination of the pure CdS and pure CdSe chemical shifts. This is in good agreement with our studied alloyed  $\text{CdSe}_{1-x}\text{S}_x$  system as exchanging replacement of S/Se bonding atomic ratio in the Cd coordination sphere along with the linear correlation chemical shift change trend.

As shown in the literature, optical properties such as absorption and photoluminescence vary with the sizes of nanoparticles, due to quantum confinement. It is well known that the NMR chemical shift is very sensitive to the chemical environment of the observed nucleus. Considering the data reported in the literature, the deshielding has been observed as the nanoparticle diameter decreases for  $\text{InP}$ <sup>[29]</sup> and  $\text{CdSe}$ <sup>[26]</sup> by  $^{31}\text{P}$  and  $^{77}\text{Se}$  NMR respectively. To the best of our knowledge, there have been no reports of corresponding  $^{113}\text{Cd}$  NMR measurements for CdSe nanoparticles. Very surprising to us, we could not detect any obviously changes of  $^{113}\text{Cd}$  NMR chemical shifts when the nanoparticle diameters change for both CdSe and alloyed  $\text{CdSe}_{1-x}\text{S}_x$  systems. We do not fully understand why the  $^{77}\text{Se}$  chemical shifts are much sensitive to size than those for  $^{113}\text{Cd}$ , but we note that  $^{77}\text{Se}$  has a much greater chemical shift range (approximately 3000 ppm) than does  $^{113}\text{Cd}$  (approximately 650 ppm).<sup>[29]</sup> One can consider that the ionic radius of  $\text{Se}^{2-}$  is much larger than that for  $\text{Cd}^{2+}$  inside the CdSe crystal lattices. It has indicated that the  $^{77}\text{Se}$  NMR chemical shifts are much sensitive than  $^{113}\text{Cd}$  NMR chemical shifts in the previous study.

## 2.6. Phase Study

The appearance of a single resonance in the  $^{113}\text{Cd}$  NMR spectra is evidence of homogeneity and not phase separation in these samples. However, we investigated the possibility of phase separation by quenching the samples with a cold ethanol and

toluene solution (1:1 volume ratio). The  $^{113}\text{Cd}$  NMR spectra of the quenched samples obviously differed from the spectra obtained for the samples prepared by slowly cooling process. Two separate peaks with small shoulders were observed for each sample, one at greater than 580 ppm and another at less than 360 ppm (Figure 9). This indicates at least two different Cd (II) nuclear chemical environments, or separate phases, present inside the quenched alloyed nanoparticles. One can speculate that the quenching process may cause a phase separation between the nanoparticle core and surface or that it may bring about surface oxidation during fast quenching in air.  $^{113}\text{Cd}$  NMR spectra of CdO and Cd-octadecene complexes show a single resonance at 382 and  $-60.5$  ppm, respectively (SI, Figure S6), which rule out the possibility of surface oxidation. Compared to the  $^{113}\text{Cd}$  NMR spectra of the slow-cooled samples, the signal above 580 ppm is assigned to Cd(II) nuclei inside the core of the nanoparticles, and the other below 360 ppm, is probably a formation of a defective phase on the particle surface or shell as a result of quick quenching. Core represents by blue and shell by light blue as shown in Figure 9. The chemical shift of greater than 580 ppm (low field peak) is assigned to the core of nanoparticles and less than 360 ppm (up field peak) assigned to the shell of nanoparticles in each quenching sample (Figure 9). Because all the chemical shifts of quenching samples greater than 580 ppm signal is well fit the equation of (1) that means the  $^{113}\text{Cd}$  NMR signals come from the same phases as these in no quenching synthesis samples (SI, Figure S7). XRD data indicate a cubic phase arises from the quenched samples rather than the hexagonal phase obtained for the slow-cooled samples (SI, Figure S8). Thus, quenching  $\text{CdSe}_{1-x}\text{S}_x$  changes the lattice pattern and causes a phase separation as well. To further demonstrate the phase separation, two separate phases of bulk CdS (yellow-brown) and bulk CdSe (black) were mixed (1:1 molar ratio) and grinded by agate until the phase separation could not distinguish by visual inspection. The  $^{113}\text{Cd}$  NMR spectrum (top spectrum in Figure 9 or SI, Figure S9) clearly shows two separate symmetric signals corresponding to those

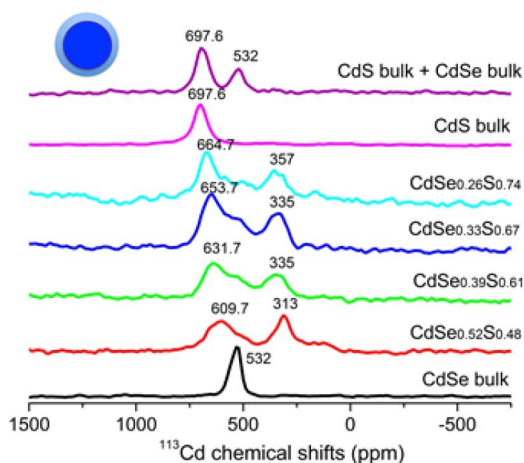


**Figure 9.**  $^{113}\text{Cd}$  NMR spectra of  $\text{CdSe}_{1-x}\text{S}_x$  ( $0 < x < 1$ ) samples prepared by the quick quenching process. Core (blue)-shell (light blue) nanoparticles formed, low field peak arises from the core and up field peak from the formed shell phase.

for pure CdS and CdSe individual, respectively. This result encourages us to believe that NMR spectra can be used to discern phase separation, and identify whether the phase is either homogeneous or heterogeneous.

## 2.7. Correlations

XRD data show that the unit cell volumes of different alloyed  $\text{CdSe}_{1-x}\text{S}_x$  nanomaterials shrink when the sulfur molar fraction increases. This is expected since the sulfur radius is less than that for selenium. A plot between the unit cell volume, determined by X-ray powder diffraction, and the corresponding  $^{113}\text{Cd}$  NMR chemical shift is both for  $\text{CdSe}_{1-x}\text{S}_x$  nanoparticles and nanobelts (SI, Figures S10–S11). This observation provides further evidence that the phase of the alloyed nanomaterials is homogeneous. It has found that this phenomenon also perfectly fit the bulk powder phases of CdS, CdSe and CdTe (SI, Figure S12). Thus,  $^{113}\text{Cd}$  NMR measurements provide another possible way to determine the unit cell volume for the alloyed  $\text{CdSe}_{1-x}\text{S}_x$  nanoparticle system.

## 2.8. Discussions

All  $^{113}\text{Cd}$  NMR spectra were measured in stationary solid state using solid state NMR facility. There is no systemic data available for series of different compositions of alloyed  $\text{CdSe}_{1-x}\text{S}_x$  nanomaterials.<sup>[27]</sup> However some data related to pure individual phase for bulk and nanoparticles, e.g., CdS, CdSe and CdTe were available and two types of chemical shift references were used, either solid  $\text{Cd}(\text{NO}_3)_2 \cdot 4\text{H}_2\text{O}$ <sup>[35,36,38,39]</sup> or 0.1 M  $\text{Cd}(\text{ClO}_4)_2 \cdot 6\text{H}_2\text{O}$  in water.<sup>[40,46]</sup> Because there is a 100 ppm difference in the chemical shifts of these two reference compounds, one must exam literature data carefully when comparing obtained values with reported values.<sup>[50,64]</sup> All our chemical shift data measured here were all referenced to 0.1 M  $\text{Cd}(\text{ClO}_4)_2 \cdot 6\text{H}_2\text{O}$  in water.

CdS and CdSe crystalline in hexagonal structure with ZnO arrangement, cadmium anisotropic nuclear magnetic shielding were observed and the order of magnitude are very similar and in small values.<sup>[46]</sup> CdTe is cubic lattice and thus no anisotropic magnetic shielding has been observed.<sup>[46]</sup> The  $^{113}\text{Cd}$  NMR spectra of these three powder samples (CdS, CdSe and CdTe) all yielded symmetric signals with the line-widths increasing according to  $\text{CdS} > \text{CdSe} > \text{CdTe}$  (SI, Figure S5) without any indication of anisotropic shielding. Our  $^{113}\text{Cd}$  NMR spectra are similar to those reported for sulfur-rich CdS nanoparticles and obviously different from those for the cadmium-rich CdS nanoparticles which displays a broad  $^{113}\text{Cd}$  spectrum pattern with many signals.<sup>[27]</sup> Indeed our alloyed  $\text{CdSe}_{1-x}\text{S}_x$  nanomaterials were all anion-rich in the initial reactants so the alloyed nanoparticle phase is a sulfur-rich system.

There is only one study of alloyed gradient  $\text{CdSe}_{1-x}\text{S}_x$  nanoparticles with varying composition from core to a few different outside shells that included  $^{113}\text{Cd}$  NMR spectroscopy, but the authors observed many  $^{113}\text{Cd}$  NMR peaks.<sup>[38]</sup> Unfortunately the compositions of the core and shells were not

determined accurately. Nevertheless, allowing for the different referencing, our NMR data are reasonably close to that reported by these authors.<sup>[38]</sup>

There has not been a careful <sup>113</sup>Cd NMR investigation of spin-lattice relaxation times ( $T_1$ ) or relaxation rates ( $1/T_1$ ) for these CdS, CdSe and CdTe semiconductive materials. We have measured <sup>113</sup>Cd  $T_1$  times for these three bulk materials and for some alloyed CdSe<sub>1-x</sub>S<sub>x</sub> nanobelts (Table 2). There are some correlations between energy gaps and their corresponding  $T_1$ s warranting further consideration. Plots energy gaps ( $E_g$ ) vs  $T_1$  are all linear with coefficients of determination  $R^2$  value 0.88223,  $E_g$  vs  $1/T_1$  with  $R^2 = 0.97665$  and  $E_g$  vs  $\log(1/T_1)$ ,  $R^2 = 0.99749$  (See SI, Figure S13). This data suggests that the materials' spin-lattice relaxation times may be related to the energy gaps.<sup>[65,66]</sup> However, little literature data is available and here only three samples were studied; more research as well as theoretical calculations are needed to ascertain whether this is a true correlation or merely coincidental.

### 3. Conclusions

In conclusion, we have demonstrated that the <sup>113</sup>Cd NMR chemical shifts of alloyed CdSe<sub>1-x</sub>S<sub>x</sub> materials are not affected by the nanoparticle size, but do change depending on the bound anion about the Cd(II) cation. A linear correlation has been observed between <sup>113</sup>Cd NMR chemical shifts and the sulfur content (*i.e.*,  $x$ ) for CdSe<sub>1-x</sub>S<sub>x</sub>, both in nanoparticles and nanobelts. Based on this correlation, we have developed a rapid, easy approach to determine the composition of the alloyed nanoscale materials utilizing <sup>113</sup>Cd NMR spectroscopy. The results for the selected system confirmed that one may determine the compositions and phase separations of semiconductor nanomaterials without destruction of the sample structures. This study expands the methodology for determining alloyed nanoparticle composition using a well-known NMR technique and it can be further applied to study semiconductor alloyed nanofilms, nanorods and nanowires as well as various types of alloyed bulk materials. In addition, the <sup>113</sup>Cd spin-lattice relaxation rate may be related to the energy gap; more examples are needed to verify this correlation. If there is indeed a correlation, then one may measure the relaxation rate and readily predict the material's energy gap.

## Experimental Section

### Materials and Methods

#### Materials

Cadmium oxide (CdO, 99.99%), selenium powder (Se, 99.9%), sulfur powder (99.98%), Cadmium perchlorate hydrate (99.999%), tri-*n*-octylphosphine (TOP, 90%), oleic acid (OA, 90%) and 1-octadecene (90%) were purchased from Aldrich. Hexylphosphonic acid (HPA) was purchased from the PolyCarbon Company. Carbon-coated copper grids (200 mesh) for preparing the TEM specimens were purchased from Electron Microscopy Sciences.

### Colloidal Synthesis of Alloyed CdSe<sub>1-x</sub>S<sub>x</sub> Nanoparticles in Solution

The alloyed CdSe<sub>1-x</sub>S<sub>x</sub> ( $0 < x < 1$ ) nanoparticles were synthesized by the modified colloidal approach.<sup>[22-23]</sup> In a typical procedure, 1.2 mmol of CdO (0.154 g) was loaded into a 100 ml two-neck air-free flask containing 2 ml oleic acid and 33 ml 1-octadecene, sealed with rubber caps and then degassed under a vacuum for 20 minutes, refilled with argon for two cycles. The flask was maintained under flowing argon and the mixture was heated to 300–320 °C with magnetic stirring. After the precursor of CdO was dissolved completely to form a clear colorless solution, a stock solution of mixed selenium (0.0474 g) and sulfur (0.1536 g) (at molar ratio of Se/S at 1/8 in Table 1) powders dissolved in 3 ml of trioctylphosphine (TOP), prepared inside a dry-glove box, was quickly injected. The crystalline alloyed nanoparticles grew at this temperature. In a similar way, the other three samples were synthesized by injected different molar ratios of a Se/S stock solution under the same conditions (see Table 1). Two cooling approaches were used after the process of nucleation: one was slowly cooling down to the room temperature, and the other was to pour the reaction solution into cold mixed solvents of methanol and toluene (1:1 volume ratio), making it rapidly quench to the room temperature. Purification was done by centrifugation and decantation, then dissolution in toluene again, then precipitation by methanol followed by a repeat of the centrifugation and decantation.

### Hydrothermal Synthesis of Alloyed CdSe<sub>1-x</sub>S<sub>x</sub> Nanobelts in Neat Ethylenediamine

The calculated amounts of sulfur, selenium and Cd(ClO<sub>4</sub>)<sub>2</sub> as shown in the Table 1 were loaded into an autoclave filled with 6 ml pure neat ethylenediamine liquid, sealed and then heated for 20 hours under magnetic stirring (the heater capacity was set to 300 °C). After the reaction finished, the heater was switched off and stirring continued until the solution slowly cooled to room temperature. The products were isolated and purified by several cycles of washing with ethanol and water with centrifugation and decantation. The purified products were dried under vacuum, collected then weighed to calculate the yields. The details of the preparations are listed in Table 1 together with the elemental analysis results.

### Characterization

The final isolated products were characterized by X-ray powder diffraction (XRD) (Rigaku Multiflex X-ray diffractometer with Cu-K $\alpha$  radiation,  $\lambda = 0.154178$  nm at 35 kV and 35 mA) and by transmission electron microscopy (TEM) (JEOL 2000 FX, with an accelerating voltage of 100 kV). In addition, UV-vis absorption spectra were recorded on a Varian Cary 100 Bio-UV-Visible Spectrophotometer. ICP mass for elemental analysis was performed by a NuPlasma Multi-Collector ICP Mass Spectrometer (MC-ICPMS). ImageJ software is an image processing program developed at the National Institutes of Health (NIH) that was used to measure the size distribution of synthesized nanoparticles based on the image obtained either from SEM or TEM microscope instrument.

### <sup>113</sup>Cd NMR Measurements

The reported <sup>113</sup>Cd NMR measurements were carried out using a Tecmag Apollo 200 MHz spectrometer (44.44 MHz) with a broadband Bruker probe. Spectra were recorded using a Hahn spin-echo pulse sequence ( $\pi/2$ - $\tau$ - $\pi$ - $\tau$ -acquisition). Spin lattice relaxation measurements were undertaken by the saturation recovery technique

using typical experimental parameters that included:  $\pi/2$  pulse length of 4  $\mu$ s; recycle delay of 30–50 s; and number of scans of 2000–4000. To obtain one spectrum requires approximately 16 hours. An aqueous solution of 0.1 M Cd(ClO<sub>4</sub>)<sub>2</sub> served as reference at zero ppm.<sup>[63]</sup> Resolution was  $\sim$ 0.3 ppm, and the spectra were recorded at room temperature. We realize that there is a new technique,<sup>[67]</sup> DNP-enhanced <sup>113</sup>Cd spin diffusion MAS NMR, that can obtain solid state <sup>113</sup>Cd NMR spectra much more quickly,<sup>[41,68]</sup> which may render practical more detailed studies.

### Supporting Information Summary

Supporting information contains the detail data of XRD, additional of <sup>113</sup>Cd NMR spectra, spin-lattice relaxation T<sub>1</sub> measurement data and process and some correlation plots as well as the measured nanoparticle diameter distributions (Table S1–S4 and Figure S1–S14).

### Acknowledgments

This work was performed at the Institute of Carbon Materials Science of Shanxi Datong University in Datong, and supported by Foundation items: National Natural Science Foundation of China (52071192), Shanxi 1331 Project Foundation for Graphene Industrialization Application Technology of Collaborative Innovation Center, Shanxi Graphene Functional Materials Engineering Technology Research Center (201705D141034), Shanxi New Carbon Functional Materials Engineering Research Center, Special talents in Shanxi Province (talents science and technology innovation) (201705D211010), Key Research Plan (Project) in Industry of Shanxi Province (201703D121037-2), Science and Technology Achievements Transformation Guide Project of Shanxi Province (201804D131041), Shanxi Science and Technology Major Project (20181102003). The authors thank Dr. Guy Bernard for his helpful comments.

### Conflict of Interest

The authors declare no conflict of interest.

**Keywords:** Nanoparticles · crystalline materials · semiconductive nanoparticles · solid state NMR.

[1] A. Henglein, *Chem. Rev.* **1989**, 89(8), 1861–1873.  
 [2] M. G. Bawendi, M. L. Steigerwald, L. E. Brus, *Annu. Rev. Phys. Chem.* **1990**, 41, 477–496.  
 [3] A. P. Alivisatos, *Science* **1996**, 271, 933–937.  
 [4] J. R. Heath, *Acc. Chem. Rev.* **1999**, 32(5), 389–396.  
 [5] C. B. Murray, C. R. Kagan, M. G. Bawendi, *Annu. Rev. Mater. Sci.* **2000**, 30, 545–610.  
 [6] M. J. Bruchez, M. Moronne, P. Gin, S. Weiss, A. P. Alivisatos, *Science*, **1998**, 281, 2013–2016.  
 [7] W. C. W. Chan, S. M. Nie, *Science* **1998**, 281, 2016–2018.  
 [8] M. E. Akerman, W. C. W. Chan, P. Laakkonen, S. N. Bhatia, E. Ruoslahti, *Proc. Natl. Acad. Sci. USA* **2002**, 99(2), 12617–12621.  
 [9] B. Dubertret, P. Skourides, D. J. Norris, V. Noireaux, A. H. Brivanlou, A. Libchaber, *Science* **2002**, 298, 1759–1762.  
 [10] X. Wu, H. Liu, J. Liu, J. Liu, K. N. Haley, J. A. Treadway, J. P. Larson, N. Ge, F. Peale, M. P. Bruchez, *Nat. Biotechnol.* **2003**, 21(1), 41–46.

[11] Y. K. Jaiswal, H. Mattoussi, J. M. Mauro, S. M. Simon, *Nat. Biotechnol.* **2003**, 21(1), 47–51.  
 [12] C. J. Murphy, *Anal. Chem.* **2002**, 74(19), 520 A–526 A.  
 [13] B. O. Dabbousi, J. Rodriguez-Viejo, F. V. Mikulec, J. R. Heine, H. Mattoussi, R. Ober, K. F. Jensen, M. G. Bawendi, *J. Phys. Chem. B* **1997**, 101, 9463–9475.  
 [14] X. G. Peng, M. C. Schlamp, A. V. Kadavanich, A. P. Alivisatos, *J. Am. Chem. Soc.* **1997**, 119, 7019–7029.  
 [15] Y. W. Cao, U. Banin, *J. Am. Chem. Soc.* **2000**, 122, 9692–9702.  
 [16] K. M. Nanif, R. W. Meulenberg, G. F. Strouse, *J. Am. Chem. Soc.* **2002**, 124, 11495–11502.  
 [17] F. V. Mikulec, M. Kuno, M. Bennati, D. A. Hall, R. G. Griffin, M. G. Bawendi, *J. Am. Chem. Soc.* **2000**, 122(11), 2532–2540.  
 [18] G. Counio, T. Gacoin, J. P. Boilot, *J. Phys. Chem. B* **1998**, 102, 5257–5260.  
 [19] A. Mews, A. Eychmuller, M. Giersig, D. Schooss, H. Weller, *J. Phys. Chem.* **1994**, 98(3), 934–941.  
 [20] R. B. Little, M. A. El-Sayed, G. W. Bryant, S. Burke, *J. Chem. Phys.* **2001**, 114, 1813–1822.  
 [21] R. E. Bailey, S.-M. Nie, *J. Am. Chem. Soc.* **2003**, 125, 7100–7106.  
 [22] E. Jang, S. Jun, L. Pu, *Chem. Commun.* **2003**, 2964–2965.  
 [23] X.-H. Zhong, M.-Y. Han, Z.-L. Dong, T. J. White, W. Knoll, *J. Am. Chem. Soc.* **2003**, 125, 8589–8594.  
 [24] X.-H. Zhong, Y.-Y. Feng, W. Knoll, M.-Y. Han, *J. Am. Chem. Soc.* **2003**, 125, 13559–13563.  
 [25] J. P. Yesinowski, (2011), *Solid State NMR of Inorganic Semiconductors*, in: J. Chan (eds) *Solid State NMR. Topics in Current Chemistry*, Vol 306. Springer, Berlin, Heidelberg, [https://doi.org/10.1007/128\\_2011\\_208](https://doi.org/10.1007/128_2011_208).  
 [26] A. M. Thayer, M. L. Steigerwald, T. M. Duncan, D. C. Douglass, *Phys. Rev. Lett.* **1988**, 60(25), 2673–2676.  
 [27] V. Ladizhansky, G. Hodes, S. Vega, *J. Phys. Chem. B* **1998**, 102, 8505–8509.  
 [28] M. Tomaselli, J. L. Yarger, M. Bruchez, R. H. Havlin, D. deGraw, A. Pines, A. P. Alivisatos, *J. Chem. Phys.* **1999**, 110(18), 8861–8864.  
 [29] M. G. Berrettini, G. Braun, J. G. Hu, G. F. Strouse, *J. Am. Chem. Soc.* **2004**, 126, 7063–7070.  
 [30] D. D. Lovingood, R. Achey, A. K. Paravastu, G. F. Strouse, *J. Am. Chem. Soc.* **2010**, 132, 3344–3354.  
 [31] S. Bjorgvinsdottir, B. J. Walder, A. C. Pinon, L. Emsley, *J. Am. Chem. Soc.* **2018**, 140, 7946–7951.  
 [32] M. P. Hanrahan, Y. Chen, R. Blome-Fernandez, J. L. Stein, G. P. Pach, M. A. S. Adamson, N. R. Neale, B. M. Cossairt, J. Vela, A. J. Rossini, *J. Am. Chem. Soc.* **2019**, 141, 15532–15546.  
 [33] P. A. W. Dean, J. J. Vittal, N. C. Payne, *Inorg. Chem.* **1987**, 26(11), 1683–1689.  
 [34] T. J. Boyle, S. D. Bunge, T. M. Alam, G. P. Holland, T. J. Headley, G. Avilucea, *Inorg. Chem.* **2005**, 44, 1309–1318.  
 [35] R. Wang, O. Calvignanello, C. I. Ratcliffe, X. Wu, D. M. Leek, Md. B. Zaman, D. Kingston, J. A. Ripmeester, K. Yu, *J. Phys. Chem. C* **2009**, 113, 3402–3408.  
 [36] C. I. Ratcliffe, K. Yu, J. A. Ripmeester, Md. B. Zaman, C. Badarau, S. Singh, *Phys. Chem. Chem. Phys.* **2006**, 8, 3510–3519.  
 [37] T. Kurihara, Y. Noda, K. Takegoshi, *J. Phys. Chem. Lett.* **2017**, 8, 2555–2559.  
 [38] J. Zhang, Q. Yang, H. Cao, C. I. Ratcliffe, D. Kingston, Q. Y. Chen, J. Ouyang, X. Wu, D. M. Leek, F. S. Riehle, K. Yu, *Chem. Mater.* **2016**, 28, 618–625.  
 [39] M. Li, J. Ouyang, C. I. Ratcliffe, L. Pietri, X. Wu, D. M. Leek, I. Moudrakovski, Q. Lin, B. Yang, K. Yu, *ACS Nano*, **2009**, 3, 3832–3878.  
 [40] M. Pentimalli, F. Antolini, E. M. Bauer, D. Capitani, T. D. Luccio, S. Vief, *Mater. Lett.* **2006**, 60, 2657–2661.  
 [41] L. Piveteau, T.-C. Ong, A. J. Rossini, L. Emsley, C. Copéret, M. V. Kovalenko, *J. Am. Chem. Soc.* **2015**, 137, 13964–13971.  
 [42] L. Piveteau, D. N. Dirin, C. P. Gordon, B. J. Walder, T.-C. Ong, L. Emsley, C. Copéret, M. V. Kovalenko, *Nano Lett.* **2020**, 20, 3003–3018.  
 [43] N. F. Ramsey, *Phys. Rev.* **1950**, 78(6), 699–703.  
 [44] J. Mason, *Chem. Rev.* **1987**, 87, 1299–1312.  
 [45] H. Nakatsuji, K. Kanda, K. Endo, T. Yonezawa, *J. Am. Chem. Soc.* **1984**, 106(17), 4653–4660.  
 [46] A. Nolle, *Z. Naturforsch. A*, **1978**, 33 A, 666–671.  
 [47] C. A. Fyre, J. M. Thomas, J. Klinowski, G. Gobbi, *Angew. Chem.*, **1983**, 95, 257–273.  
 [48] A.-R. Grimmer, R. Peter, E. Fechner, G. Moldegney, *Chem. Phys. Lett.* **1981**, 77, 331–335.  
 [49] E. Lippmaa, M. Mägi, A. Samoson, G. Engelhardt, A.-R. Grimmer, *J. Am. Chem. Soc.* **1980**, 102(15), 4889–4893.



- [50] P. G. Mennitt, M. P. Shatlock, V. J. Bartuska, G. E. Maciel, *J. Phys. Chem.* **1981**, *85*(14), 2087–2091.
- [51] P. L. Goggin, R. J. Goodfellow, D. M. McEwan, A. J. Griffiths, K. Kessler, *J. Chem. Res.* **1979**, (S) 194–195, (M) 2315–2343.
- [52] W. Freeman, P. S. Pregosin, S. N. Sze, L. M. Venanzi, *J. Magn. Reson.* **1976**, *22*, 473–478.
- [53] S. J. S. Kerrison, P. J. Sadler, *J. Chem. Soc. Dalton Trans.* **1982**, 2363–2369.
- [54] J. J. Pesek, W. R. Mason, *J. Magn. Reson.* **1977**, *25*, 519–529.
- [55] A. V. Von Zelewsky, *Helv. Chim. Acta.* **1968**, *51*, 803–807.
- [56] Ö. Gröning, T. Drakenberg, L. I. Iding, *Inorg. Chem.* **1982**, *21*(5), 1820–1824.
- [57] R. G. Kidd, R. J. Goodfellow, In *NMR and the periodic table*; R. K. Harris, B. E. Mann, Academic; London, **1978**; Chap. 8.
- [58] S. J. S. Kerrison, P. J. Sadler, *J. Magn. Reson.* **1978**, *31*, 321–325.
- [59] P. S. Pregosin, M. Kretschmer, W. Preetz, G. Rimkus, *Z. Naturforsch. B* **1982**, *37B*, 1422–1424.
- [60] H. J. Jakobsen, P. D. Ellis, *J. Phys. Chem.* **1981**, *85*, 3367–3369.
- [61] G. Ma, A. Fischer, R. Nieuwendaal, K. Ramaswamy, S. E. Hayes, *Inorg. Chim. Acta* **2005**, *358*, 3165–3173.
- [62] G.-B. Ma, A. Ilyukhin, J. Glaser, I. Tóth, L. Zékány, *Inorg. Chim. Acta* **2001**, *320*, 92–100.
- [63] R. K. Harris, B. E. Mann, *NMR and the Periodic Table*, **1978**, Academic Press, New York, p264.
- [64] B. A. Demko, R. E. Wasylshen, *Dalton Trans.*, **2008**, 481–490.
- [65] M. Shroyer, J. K. Furdyna, A. I. Ryskin, W. W. Warren, Jr, *Physica B+C* **1999**, *273–274*, 852–855.
- [66] D. Yu, K. Du, J. Zhang, F. Wang, L. Chen, M. Zhao, J. Bian, Y. Feng, Y. Jiao, *New J. Chem.* **2014**, *38*, 5081–5086.
- [67] V. K. Michaelis, R. G. Griffin, B. Corzilius, S. Vega, *Handbook of High Field Dynamic Nuclear Polarization*, Wiley and Sons Ltd. **2020**, pp. 472.
- [68] M. P. Hanrahan, Y. Chen, R. Blome-Fernandez, J. L. Stein, G. F. Pach, M. A. S. Adamson, N. R. Neale, B. M. Cossairt, J. Vela, A. J. Rossini, *J. Am. Chem. Soc.* **2019**, *141*, 15532–15546.

---

Manuscript received: August 3, 2020

Revised manuscript received: September 3, 2020